DISCLAIMER NOTICE

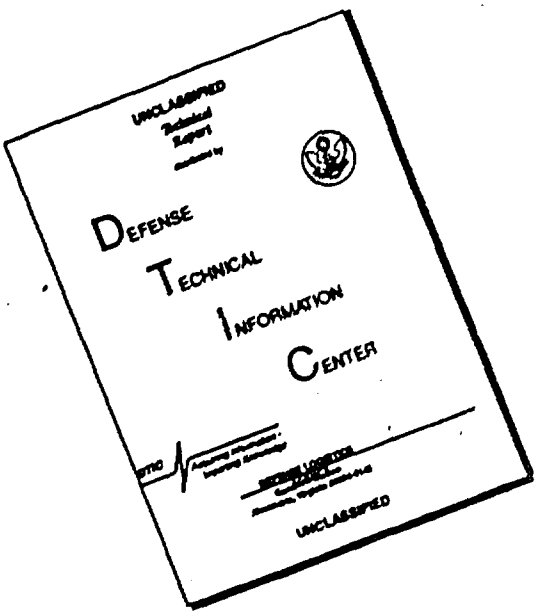

THIS DOCUMENT IS BEST QUALITY AVAILABLE. THE COPY FURNISHED TO DTIC CONTAINED A SIGNIFICANT NUMBER OF PAGES WHICH DO NOT REPRODUCE LEGIBLY.

BOEING

SPACE PROTON DOSES AT POINTS WITHIN THE HUMAN BODY*

by

David L. Dye**

SEATTLE, WASHINGTON

SPACE PROTON DOSES AT POINTS WITHIN THE HUMAN BODY*

by

David L. Dye**

A paper presented to the

Symposium on Protection Against Radiation

Hazards in Space,

November 5-7, 1962

Gatlinburg, Tennessee.

*This report is a condensed version of a Boeing Document yet to be released, D2-90106, with the same title.

**Applied Physics Section, Aero-Space Division, The Boeing Company, Seattle, Washington.

SPACE PROTON DOSES AT POINTS WITHIN THE HUMAN BODY

David L. Dye
The Boeing Company

Abstract

Distribution patterns of absorbed dose influence the radiation response of a mammalian system, because of differing radiosensitivities of different organ systems. In a man exposed to space radiations; e.g., an astronaut, body self-shielding produces nonuniform dose distributions which depend upon external shielding configurations and the incident radiation parameters. In this paper are presented the doses at twelve specific points in the body of a seated man exposed to isotropic incident space protons, where the man is inside various thicknesses of external vehicle shell shielding. The body points, selected for their radiobiological interest, are in (or on) sternum, chest skin, femur, spinal column, eye, central gut, and a series at various lateral depths on the waist. The protons reaching these specific points from all directions traverse tissue thicknesses that were determined from scale drawings of a statistically standard man (75-percentile). The proton penetration, secondary radiation generation, and total dose delivered to each specific body point was calculated using an IBM (Fortran) computer code.

For feasibly thin aluminum shields and typical spectra, the secondary dose is a small fraction of the total proton dose for most of the body points. The doses at a given point vary with both spectral shape and external shielding, as well as point to point. Power law spectra, $E^{-n}dE$, normalized to one proton/cm^2-sec of $E > 100$ Mev, with $2 \leq n \leq 5$, and the Freden and White trapped proton spectrum, were considered. Resulting dose values for $n = 3$ to 4 (a

typical solar flare-associated proton spectrum) vary from about 10^{-4} to 10^{-8} rad/proton/cm^2 > 100 Mev for the various body points for a 1 gm/cm^2 external shield, and from 10^{-7} to 10^{-8} rad/proton/cm^2 > 100 Mev for a 10 gm/cm^2 external shield.

Introduction

Dose distribution patterns in a biological system have an important influence on the radiation effects in that system. In the human body exposed to a typical space proton environment, there is some self-shielding that reduces the body interior doses with respect to the skin doses and thus affords some measure of radiation protection. Previous studies have been made of the depth-dose patterns resulting from several simple proton spectra impinging on slab shields and penetrating into tissue slabs.[1,2] These early results show the dependence of depth-dose on spectral shape and exterior shielding, but the simplified geometry used leaves one still wondering just what the absorbed doses are inside a biologically interesting shape such as the human body.

The earlier results were calculated by means of an IBM 7090 computer code.[2] A slightly modified version of this same program was used in part of the present calculation. A principal feature of the present program is that it calculates a series of dose values due to penetrating protons in a set of slab geometries, then sums these dose values, weighted as necessary by the fractional solid angles subtended by each slab problem, to obtain the proper total dose at an interior point. For the work here reported, the seated human (75-percentile male) body was used, with various spherical shells around it. Doses were computed at a number of body-interior points: femur, sternum,

---

1. D. L. Dye and J. C. Noyes, Biological Shielding for Radiation Belt Particles, J. Astron. Sci. VII, 64 (1959).

2. D. L. Dye and G. Butler, Computer Calculations of Doses from Protons in Space, J. Astron. Sci. IX, 63-71 (1962).

backbone, eye lens, central gut, and at waist level.[3] The results of these computations are tabulated here and show a dependence on spectral and shielding parameters similar to the earlier results. However, these values now represent useful doses (per isotropic incident proton/cm^2 of E > 100 Mev) at the specific body points. If the incident isotropic flux and spectrum is known exactly--an unlikely eventuality--then the proton ionization dose at any of these points may be known accurately.

The dose due to secondaries generated in nuclear interactions has been estimated variously [4,5] but it is small for thin shields. A computer program has been developed to determine the tissue doses due to the secondaries generated by the incident primary protons in the shielding material. The secondary component includes inelastic scattering-produced gamma rays, low-energy evaporation nucleons, and high-energy knock-on nucleons. Part of the tertiary neutron and gamma effects were included, by adding the secondary proton spectrum to the primary at every point, so the total was used in interior sublayers. The results justify the usual procedure of neglecting the secondaries from incident space protons of typical energy spectra.

The Computer Programs

Primary Dose Code

Spectral Modification. In the present version of the primary proton dose calculation, an incident proton spectrum is degraded through shielding layers according to formulas 1 to 3 of Ref. 2. However, instead of interpolating between tabulated range-energy points, as was

---

3. D. L. Dye, A Geometrical Analysis of the Seated Human Body for Use in Radiation Dosage Calculations, The Boeing Company, D2-90107, (1962).

4. R. I. Allen, et al., Shielding Problems in Manned Space Vehicles, Lockheed Aircraft Corp., NT-140, (1961).

5. R. K. Wilson, et al., A Study of Space Radiation Shielding Problems for Manned Vehicles, General Dynamics Corp., FZK-144 (1962).

done in Ref. 2, we have made a least squares fit to those tables[6] to obtain analytic expressions for proton range as a function of energy and energy as a function of range. Thus, the proton range function is defined empirically to be:

$$\mathrm{RNGEF(E)} = \exp(A1 + A2 \log E + A3 \log^2 E), \tag{1}$$

and the proton energy function is (by quadratic inversion):

$$\mathrm{ENGYF(R)} = \exp\left[\frac{-A2 + \sqrt{A2^2 - 4A3(A1 - \log E)}}{2A3}\right], \tag{2}$$

where E is proton energy, R is proton range, and the A's are coefficients of the fit which depend on the shielding material. Equation 1 was chosen as the form to which to fit by least squares the range-energy tables because range is approximately a power law function of energy; that is,

$$R = kE^n, \tag{3}$$

with k and n slowly varying functions of E over the range of interest, $1 \lesssim E \lesssim 1{,}000$ Mev.

Use of an analytic range function provides simply for the solution to the spectral modification with penetration into shielding material. It also allows one readily to compute the output spectrum on a specified energy grid, so that spectra are easily added at an interior point.

If a monodirectional proton spectrum P(E)dE is incident on a shield layer of thickness X, then the penetrating spectrum P'(E')dE' may be computed by means of the recipe:

$$E' = \mathrm{ENGYF(RNGEF(E) - X)}, \tag{4}$$

$$P'(E')dE' = P(E)dE(dE'/dE), \tag{5}$$

and

$$(dE'/dE) = \frac{(dR/dE)_E}{(dR/dE)_{E'}} \tag{6}$$

---

6. M. Rich and R. Madey, Range Energy Tables, UCRL-2301 (1954)

where the subscripts mean that the derivative is evaluated at E and E', respectively.

In the present IBM code, an output energy grid E'(K) is specified, so the E(K) values needed to obtain it are computed by Eq. 4. Then the incident specified spectrum P(K) is rearrayed, by interpolation, onto this input energy grid. Then the "energy spread factor", determined by Eq. 6, is multiplied into the spectrum P to obtain the output spectrum P' arrayed on the specified output energy grid E'(K), according to Eq. 5.

This spectrum degrading process is repeated for each layer of shielding material until the point of interest for dose calculation is reached. The actual dose computation is done as it was earlier in versions of this code; namely, by:

$$\text{DOSE} = \int_{1}^{1{,}000\ \text{Mev}} P'(E')\ \text{DOSF}(E')\ dE' \qquad (7)$$

where DOSF(E) is proportional to dE/dX for tissue.

Vehicle Analysis. It is desired to compute a dose absorbed by some material such as tissue, within a complicated arbitrary shielding configuration such as a space vehicle or a human body, due to an arbitrary angular distribution of incident protons. The way this is done may be seen by referring to Fig. 1. Briefly, the three-dimensional material configuration is analyzed in a large number of one-dimensional problems, so that the code just described can solve the three-dimensional problems.

Looking outward from an interior point P in all directions, one sees various solid angular regions $\Delta\Omega$, over each of which the shielding layers are approximately the same. If the radiation reaching P is direct, or primary and unscattered, then we may approximate the dose at P by the sum:

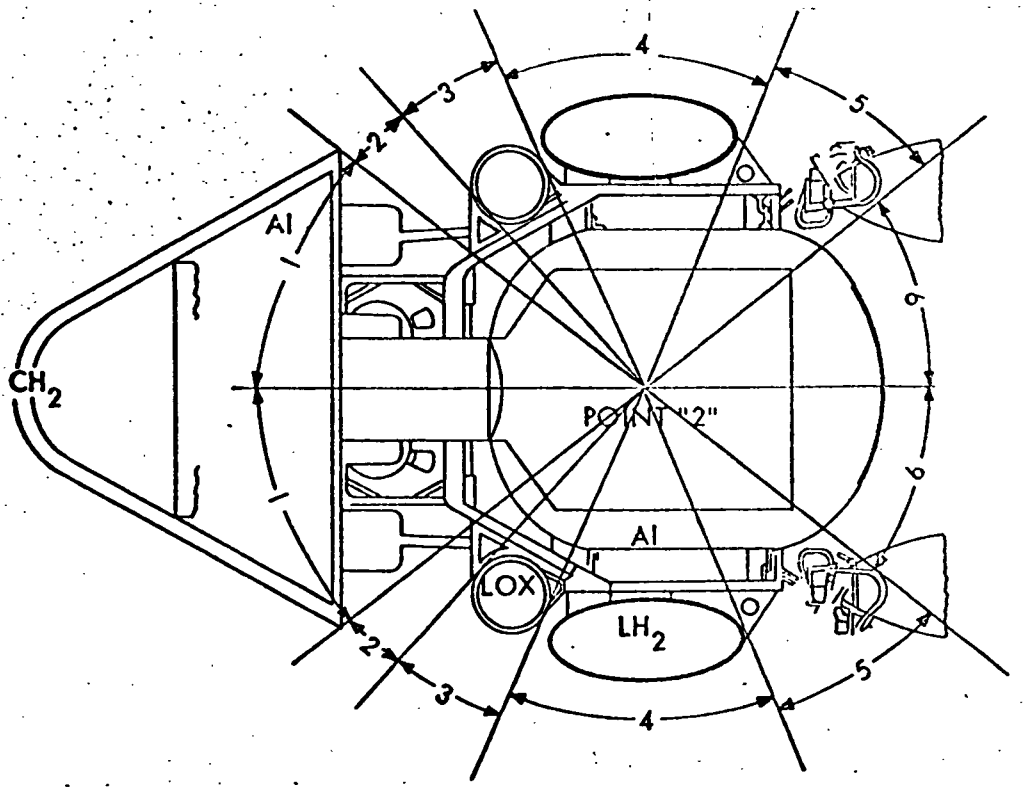

REGION	FRACTIONAL SOLID ANGLE	SHIELDING IN REGION
1	.10	3" CH_2 +4.7" Al
2	.07	1.25" Al
3 (with fuel)	.14	.02" Al +15" O_2 +1.5" Al
3 (without fuel)	.14	1.52" Al
4 (with fuel)	.4	.02" Al +18" H_2 +1.6 Al
4 (without fuel)	.4	1.62" Al
5	.13	2.2" Al
6	.18	3.1" Al

FIGURE 1

TYPICAL SPACE VEHICLE SHIELDING THICKNESS ANALYSIS

$$DOSE(P) = F \sum_{IP=1}^{NP} \left[DOSE(S_{IP})\right] \left[ANG(IP)\right] \left[\Delta\Omega_{IP}\right], \qquad (8)$$

where: $DOSE(S_{IP})$ is the absorbed dose computed behind a layer shield S_{IP},

S_{IP} represents the one-dimensional shielding configuration of whatever layers, materials, and thicknesses specified for the solid angular region indexed by IP,

ANG(IP) is the fraction of the flux coming from the IP direction, calculable from the angular distribution of the incident radiation, and normalized to be a constant unity value for isotropic flux,

F is the incident flux assumed suitably normalized,

$\Delta\Omega_{IP}$ is the fractional solid angle subtended about the point of interest P by the constant shielding region IP, and

NP is the total number of such regions needed to complete the full solid angle, so that the vehicle shielding is analyzed into sufficiently small angular regions to obtain the desired accuracy.

In Fig. 1, six regions were chosen to illustrate the concepts, but an actual analysis might use more. In the body point results reported here, 15 to 25 regions were used in most cases. It was found that little change in the final dose answer is obtained with larger numbers of subregions than this; that is, the dose calculation converges with relatively large $\Delta\Omega$ values for practical cases.* Equation 8 describes the method of calculating a dose to an interior point due to incident primary, straight-through, radiation of arbitrary incident angular

*See the paper by J. W. Keller, this symposium, for some further comments on the need for an adequately fine analysis.

distribution. Because in practice a space vehicle is likely to be drifting or slowly tumbling, the results computed and here reported are for isotropic distributions. Also, DOSE(S) was normalized to one proton/cm^2 of energy E > 100 Mev (for power law spectra), so the normalization of F, incident flux, must be compatibly defined.

Thus, in a vehicle shielding design problem, a geometrical analysis is made of the proposed design to determine a number of "constant-shielding" regions about an interior point. The dose at that point is calculated, one-dimensionally, for each of the constant-shielding regions and the weighted sum, Eq. 8, is performed using the dose values and the fractional solid angles for each region. The vehicle analysis part is a drafting board problem, and can be done quickly and with adequate accuracy for most practical vehicle configurations. But the power of this method is in the fact that any complex arrangement can be analyzed in these terms. The dose results presented here apply to specific points inside a very complex shielding arrangement--the tissue of the human body.[3]

Secondary Dose Code

Secondary Radiation Components. In addition to the dose due to primary penetrating protons, there is some energy deposition by the secondary radiations generated by the incident protons. These secondaries include gamma rays, and evaporation and knock-on nucleons. The neutrons and protons are generated in nuclear reactions where an incident proton excites a shield material nucleus. Some neutrons and protons of high energy (up to about the incident proton energy) can theoretically be produced. The bulk of the secondary neutrons and protons, perhaps with ten times the intensity of the high energy tail, are produced by evaporation from the excited nucleus. These evaporation nucleons are generated isotropically and have energies of 5 to 25 Mev, and proton numbers are roughly one half the neutron numbers. The statistical theory of the nucleus, which formally describes the excitation and evaporation processes, is invalid for the low atomic number

nuclei, such as carbon or aluminum, so the proton interaction probabilities were not computed using that theory. Rather, experimental data[7] were used to estimate the total neutron production probabilities as a function of incident proton energy.

Gamma rays emerge from excited nuclei, having energies depending on the specific nuclei and excitation levels. The excitation may be residual from a higher energy nucleon-producing interaction, or it may be from an inelastic scattering process in which the incident proton loses a relatively small amount of energy to the nucleus. From either cause, a discrete gamma ray spectrum results from the passage of high energy protons through matter.[8]

The secondary dose code was developed to compute, for all three components, the secondary fluxes and spectra generated in successive layers of the shielding, the secondary flux and spectra penetrating through the material between the generation layer and the interior point of interest, and the total absorbed dose at the interior point.

Description of the Code. The secondary code will not be described here in detail, as it is to be reported elsewhere.[9] Only enough discussion will be given to indicate how the preliminary results depend on the assumed secondary radiation production data, since these data are likely to be better known as more nuclear physics research is done. Then, presumably, better results will be obtained.

---

7. W. E. Crandall and G. P. Millburn, Neutron Production at High Energies, J. Appl. Phys. 29,698 (1958).

   See also R. Wallace and C. Sondhaus, (especially Figs. 12-16) this symposium, and UCRL-10439.

8. R. Madey, A. G. Duneer, Jr., and T. J. Krieger, Gamma Dose from Solar Flare Protons Incident on an Aluminum Shield, Trans. Am. Nuc. Soc. June 1962 meeting.

9. D. L. Dye, Space Proton Doses at Points Within the Human Body, The Boeing Company, D2-90106 (1962).

GENERATION AND TRANSMISSION OF SECONDARY RADIATIONS

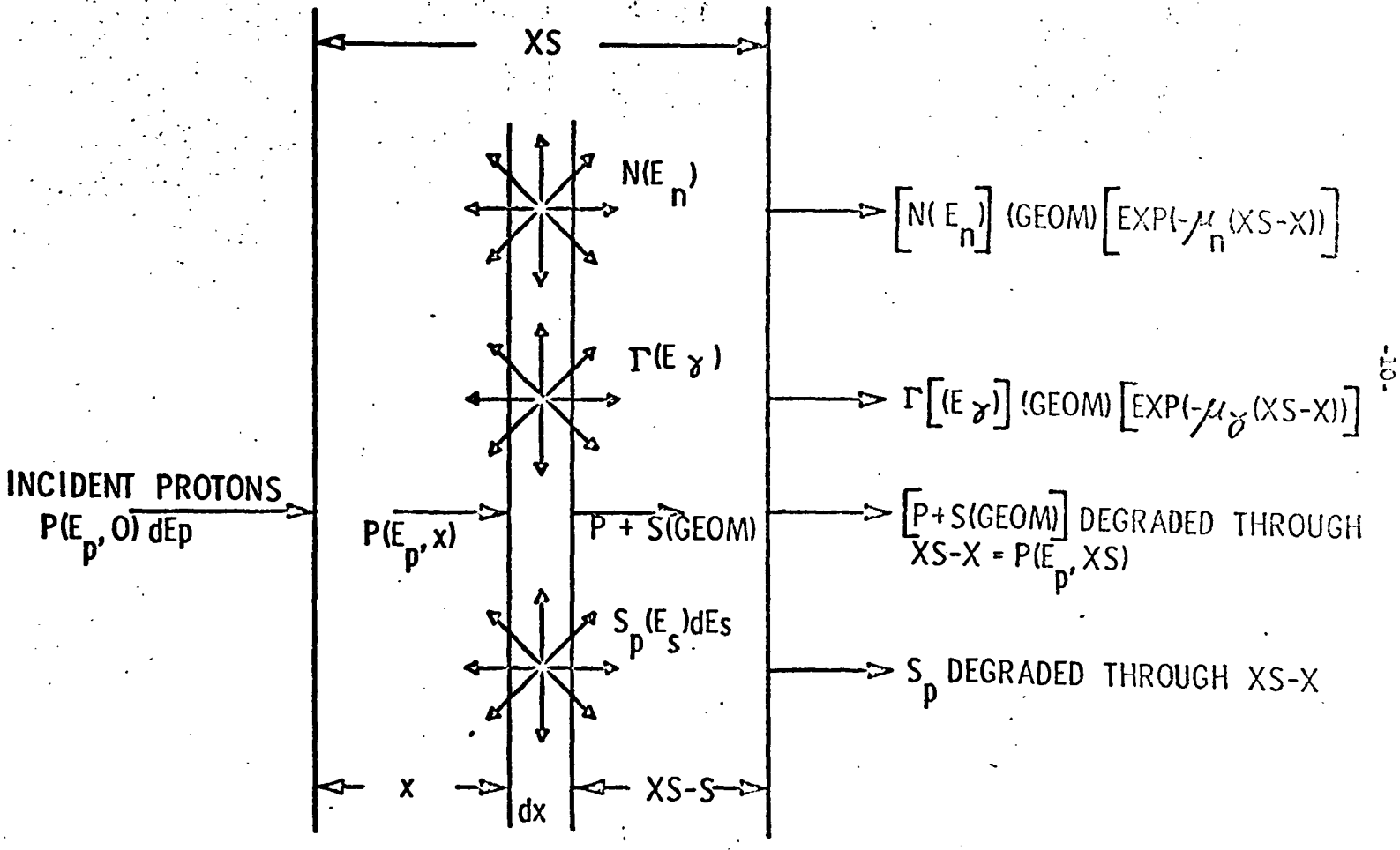

FIG. 2

Consider a layer of shielding material, Fig. 2, of total thickness XS. At a depth X, in a layer dX thick, the secondary radiation is being generated according to:

$$N(E_n) = \frac{6 \times 10^{23} dX}{A} \int P(E_p,X)\ XNMULT(E_p,E_n)\ \sigma_n(E_p)\ dE_p, \qquad (9)$$

$$\Gamma(E_\gamma) = \frac{6 \times 10^{23} dX}{A} \int P(E_p,X)\ XGMULT(E_\gamma)\ \sigma_\gamma(E_p)\ dE_p, \qquad (10)$$

and

$$S_p(E_s)E_s = \frac{6 \times 10^{23} dX}{A} \int P(E_p,X)\ XPMULT(E_p,E_s)dE_s\ \sigma_s(E_p)\ dE_p. \qquad (11)$$

Where:

A is atomic number of the shield material,

$N(E_n)$ is the flux of neutrons generated in an energy group having energy E_n,

$\Gamma(E_\gamma)$ is the flux of photons generated having energy E ,

$S_p(E_s)dE_s$ is the differential energy distribution of secondary protons generated having energy E_s to $E_s + dE_s$,

$P(E_p,X)dE_p$ is the proton energy spectrum at depth X, the flux having energy between E_p and $E_p + dE_p$,

$XNMULT(E_p,E_n)\ \sigma_n(E_p)$ is the yield of neutrons having energy E_n, per incident unit flux of protons having energy E_p,

$XGMULT(E_\gamma)\ \sigma_\gamma(E_p)$ is the yield of gamma rays having energy E_γ (due to inelastic scatter or other processes) produced per incident unit proton flux of Energy E_p. XGMULT depends primarily on the nuclear levels of the struck nucleus, while σ_γ is the cross section for an interaction,

$XPMULT(E_p,E_s)dE_s\ \sigma_s(E_p)$ is the differential yield of secondary protons having energy E_s to $E_s + dE_s$ from processes induced by incident protons of energy E_p.

The multiplicity factors (XNMULT, XGMULT, XPMULT) are normalized to one "particle" produced so that experimentally determined total yield cross sections may be used.[7,10]

---

10. T. Watasuki et al., Gamma Rays from Several Elements Bombarded by 10 and 14 Mev Protons, J. Phys. Soc. Japan 15, 1141 (1960).

A geometrical weighting factor (GEOM) is assigned to the radiation generated in any given material layer. This factor depends upon the angular distributions of the secondaries and upon the relative sizes of the vehicle shield and the dose point of interest. The fraction of the secondaries produced in a given sublayer within the shielding that is directed toward the interior dose point is given by multiplying N_s, Γ_s, or S_p by GEOM for that layer.

The neutrons and gamma rays are assumed to be absorbed by intervening shielding according to exponential laws. The protons generated in dX are added to $P(E_p, X + dX)dE_p$. (This is the reason we needed the differential energy distribution for $S_p(E_p)$). Thus, the spectrum for the next dX is enhanced by the secondary protons generated in previous sublayers.

In the actual code computation, the layer XS thick is broken up into NSL finite-thickness sublayers, where NSL is determined by a specified maximum sublayer thickness, except that NSL never exceeds another specified parameter, NSUBL. This last restriction saves computer time for thick shields.

The absorption of the neutrons and gammas is carried through all intervening shielding layers to the dose point inside, and the dose there calculated using well-known dose conversion factors. The code is dimensioned for 10 different materials and/or layers. The secondary protons are also carried through the intervening shielding separately from the total (primary plus secondary) proton flux, so as to show secondary proton dose separately. For this, the proton spectrum modification and dose code described in the previous section is used. After the absorbed doses, in rads, are computed at the interior point for each secondary component, these doses are individually converted to biological dose, in rem, by multiplying by the appropriate, specified, RBE. The individual component, as well as the total, secondary biodose is then read out. Finally, the weighted sum, Eq. 8, is done to obtain total dose from all directions at the point.

Data Used in the Secondary Dose Computation. In addition to the proton range-energy tables used in the primary dose computation, a number of nuclear and other parameters are needed in the secondary code. These include: the yield cross sections σ_n, σ_γ; the multiplicities XNMULT, XPMULT, and XGMULT; the discrete gamma ray energies generated in the specific shielding materials, designated EGAM; the gamma and neutron absorption coefficients and dose conversion factors for these energies; the angular distribution factors, GEOM, for each layer; and the maximum sublayer thickness, XLMAX, for each material. Neutron yield cross sections were found from the empirical relation

$$\sigma_n = C_1 E^{0.4}$$

which fits the experimental data[7] for aluminum and carbon (assumed the same as tissue) with $C_1 = 0.07$ and $C_1 = 0.035$, respectively. (For iron, $C_1 \simeq 0.3$.) Gamma ray yield cross sections and energies were also inferred from reported experiments [10,11] and the σ_γ values used are plotted, along with σ_n, in Fig. 3. Two different σ_γ curves were used, one in which σ_γ approaches σ_{total} at high energies, and one in which it is held constant at its low energy maximum (~ 2 barns) at high energies. This latter case is labelled "upper limit". The inelastic scatter gamma ray energies, EGAM, and multiplicities, XGMULT, for aluminum and tissue, and the NBS Handbook dose conversion coefficients, are given in Table 1.

The secondary nucleon energy distributions are somewhat less well known, and as better data become available, better dose values can be obtained by using them in this code. For the present calculation, an evaporation hump ranging from 5 to 25 Mev for secondaries was assumed for all incident proton energies above 25 Mev, and a high-energy tail was assumed to extend out to 0.5 the incident proton energy,

---

11. G. Schrank et al., Inelastic Scattering of 17-Mev Protons, Phys. Rev. 127, 2159 (1962). This paper gives many references to experimental determinations.

Table 1. Gamma Ray Energies, Multiplicities, and Dose Coefficients Assumed for the Secondary Dose Computation

Material	EGAM (Mev)	XGMULT	DOSGAM (Tissue) (rad/proton/cm^2)
Aluminum	1.4	0.45	4.8×10^{-9}
	2.2	0.19	4.0×10^{-9}
	3.0	0.25	3.5×10^{-9}
	5.0	0.08	3.3×10^{-9}
	8.0	0.03	3.2×10^{-9}
Tissue	4.4	0.88	3.0×10^{-9}
	6.1	0.06	2.9×10^{-9}
	7.0	0.06	2.9×10^{-9}

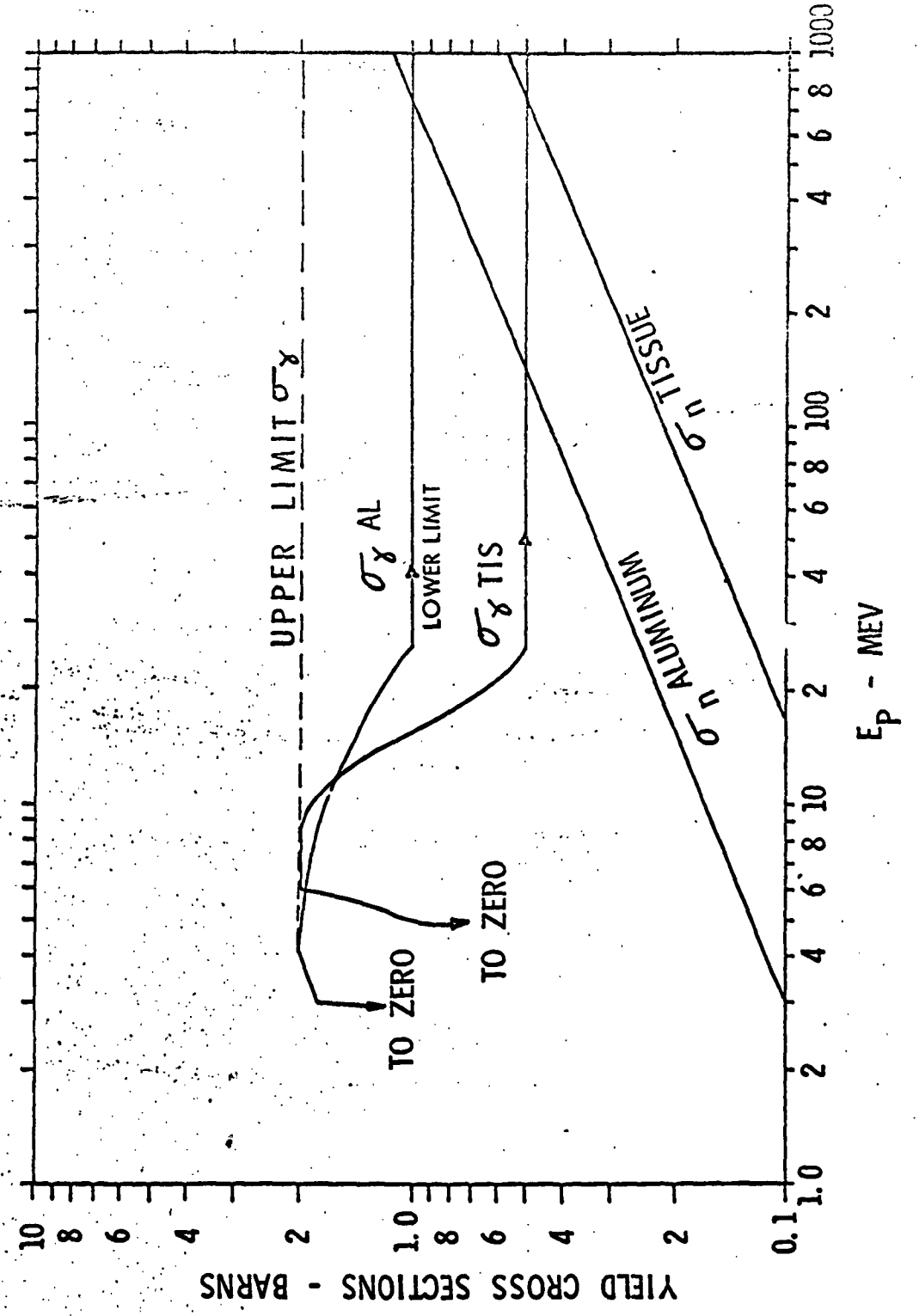
YIELD CROSS SECTIONS - BARNS
10
8
6
4
2
1.0
8
6
4
2
0.1
1.0
2
4
6
8
10
2
4
6
8
100
2
4
6
8
1000
E_p - MEV
UPPER LIMIT σ_γ
σ_γ AL
LOWER LIMIT
σ_γ TIS
TO ZERO
TO ZERO
σ_n ALUMINUM
σ_n TISSUE

FIGURE 3

containing about 10 percent of the total secondary nucleons.* The secondary spectrum was normalized, for each incident proton energy in the integration of Eq. 11, to one nucleon over the whole energy range $1 < E_s < E_p/2$. More detail is given elsewhere.[9]

The GECM factors were assumed to be constant for each shielding layer, and were taken as 0.5 for both outer aluminum and inner tissue layers in the results to be given here.

Human Geometry

The absorbed dose at each of several points in a seated astronaut is desired. The points of specific interest are those that are parts of radiosensitive physiological systems, such as hematopoetic and spinal marrow, gut, and eye lens. Twelve such body points were chosen, located as indicated in Table 2, on a 75-percentile seated man. This body geometry is based on data given[12] in an anthropometric study of Air Force personnel. (Seventy-five percent of the men had smaller body measurements than those used.) Scale drawings of this composite astronaut's body were made and used to determine the tissue thicknesses around each of the selected body points in all directions.[3] For each specific body point listed in Table 2, this descriptive geometry problem was solved; the point is taken as the center of a large sphere on which isothickness contours are projected. These contours mark out a set of solid angular regions; a region's projected area on the sphere divided by the total sphere area is the fractional solid angle of that region. Depending on the accuracy required, one may choose any set of regions to define the fractional solid angles for the human geometry problem.

The isothickness contours are obtained by drawing a series of cross sectional views of the body at different angles ϕ from the

---

12. Hertzberg, Daniels, and Churchill, Anthropometry of Flying Personnel--1950, WADC Technical Report 52-321 (1954).

*The form of this secondary nucleon distribution is not unlike that given in this symposium by Dr. K. Strauch as a "hypothetical particle spectrum", built-up on the high energy end to account for secondary angular distributions.

TABLE 2. DESCRIPTION OF BODY POINTS ANALYZED

BODY POINT	LOCATION	SYMBOL
CENTRAL GUT	10 CM UP FROM SEAT, AND 10 CM FORWARD FROM BACK OF SEAT.	GUT
CHEST CENTER	ON THE SKIN SURFACE, 55 CM UP FROM SEAT.	CHEST 0
CHEST CENTER	2 CM IN FROM THE SKIN, IN STERNUM, 55 CM UP FROM SEAT, NEGLECTING LUNGS.	CHEST 2
CHEST CENTER	2 CM DEEP, IN STERNUM, AS BEFORE, TAKING ACCOUNT OF AIR IN LUNGS.	CHEST 2 L
SPINAL CORD REGION	55 CM UP FROM SEAT, 2 CM DEEP IN BODY.	BACK 2
FEMUR	LEG CENTER, 38 CM FORWARD FROM BACK OF SEAT, 9 CM UP FROM SEAT LEVEL (NEGLECTING BONE).	FEMUR
FEMUR	SAME POINT AS BEFORE, TAKING ACCOUNT OF BONE STRUCTURE	FEMUR B
EYE LENS	RIGHT EYE SURFACE, NEGLECTING FACIAL AND CRANIAL BONY STRUCTURE.	EYE
WAIST, RIGHT SIDE	ON THE SKIN, 25 CM UP FROM SEAT LEVEL.	WAIST 0
WAIST, RIGHT SIDE	25 CM UP FROM SEAT LEVEL, 1 CM IN FROM SKIN, ON THE MID-SAGGITAL LINE.	WAIST 1
WAIST, RIGHT SIDE	25 CM UP FROM SEAT LEVEL, 4 CM IN FROM SKIN, ON THE MID-SAGGITAL LINE.	WAIST 4
WAIST, RIGHT SIDE	25 CM UP FROM SEAT LEVEL, 6 CM IN FROM SKIN, ON THE MID-SAGGITAL LINE.	WAIST 6
WAIST, RIGHT SIDE	25 CM UP FROM SEAT LEVEL, 8 CM IN FROM SKIN, ON THE MID-SAGGITAL LINE.	WAIST 8

anterior-posterior plane; and by drawing a series of horizontal cross sectional views at various planes above and below the point of interest. A tissue thickness is then obtained by determining the true distance from the point to the body surface along every (latitude) direction θ in the ϕ plane. Figure 4 illustrates the method for a specific point. The result of this descriptive geometry problem is a map on the projection sphere showing lines of constant tissue thickness between the point of interest and the body exterior along the θ, ϕ direction. Figure 5 shows a typical isothickness contour for a body point, in the spinal column. In this procedure, the human body is assumed to be a homogeneous tissue mass except for certain cases below.

Conceptually simple, but computationally tedious, extensions of the interior body point dose calculations for the STERNUM, FEMUR, WAIST 4, and EYE LENS positions were also analyzed with slight geometric variations. These variations were intended: (1) to solve more realistic problems that include bones and lung absorption effects, (2) to give an idea as to the dose error made in neglecting bones and lungs; i.e., in assuming the body to be homogeneous, (3) to assess the shielding effectiveness of partial body shielding built in as a chair, and (4) to assess the effect of goggles in eye protection.

Incident Proton Spectra

Five different incident proton spectra were considered; four having power law forms, the other approximating the Van Allen belt spectrum. The power law forms, normalized to one proton/cm^2 of E > 100 Mev, are given by:

$$N(E)dE = (n - 1)(100)^{n-1} E^{-n} dE \text{ for } 20 \text{ Mev} \leq E \leq 1{,}000 \text{ Mev}$$

for the parameter n with values 2, 3, 4, and 5. They are flat at the 20 Mev value for the interval $1 \leq E \leq 20$ Mev. The Van Allen spectrum is normalized to one proton/cm^2 of $E > 40$ Mev, and has an E^{-2} form above 100 Mev, with the lower energy part of Hess's theoretical form matched to it at 100 Mev.

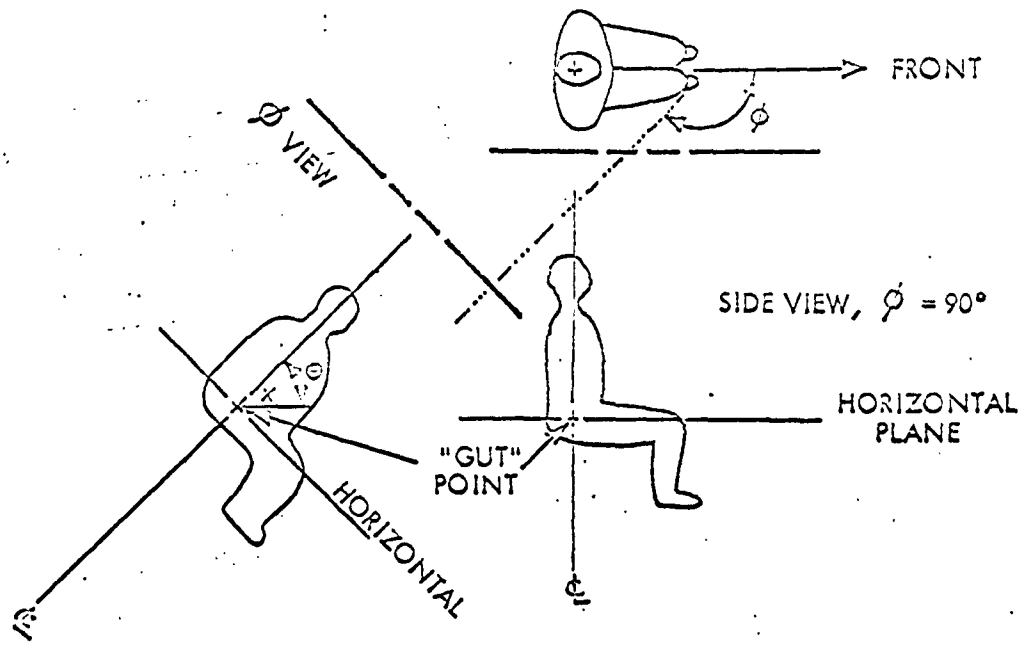

℄ IS VERTICAL AXIS, PASSING THROUGH THE POINT OF INTEREST

ϕ IS LONGITUDE ANGLE

Θ IS LATITUDE ANGLE

x IS THICKNESS, A FUNCTION OF θ AND ϕ FOR THIS POINT

FIGURE 4

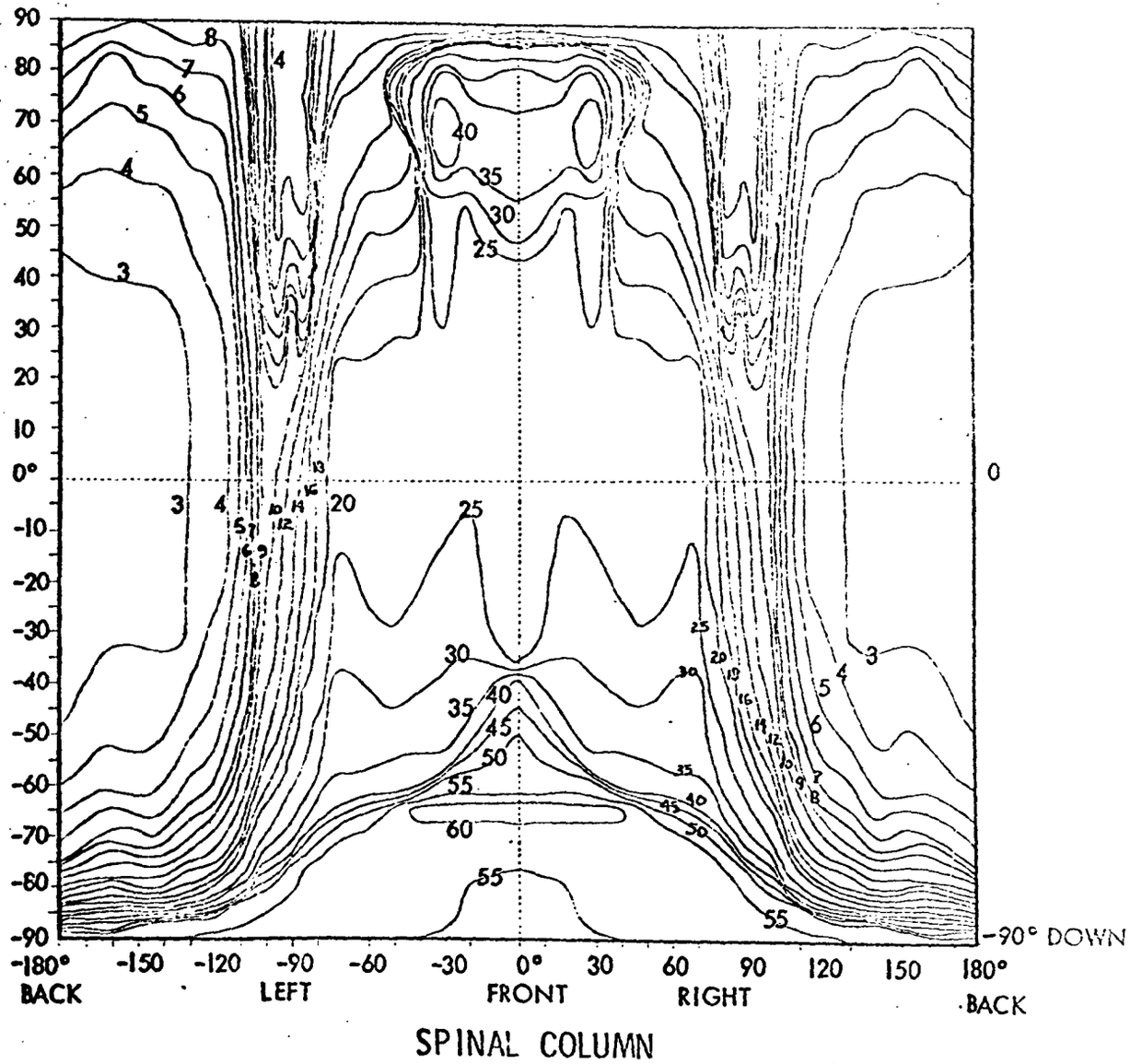
90
80
70
60
50
40
30
20
10
0°
-10
-20
-30
-40
-50
-60
-70
-80
-90
0
-90° DOWN
-180° -150 -120 -90 -60 -30 0° 30 60 90 120 150 180°
BACK
LEFT
FRONT
RIGHT
BACK
SPINAL COLUMN

FIGURE 5

Dose Results

Figure 6 shows the penetrating primary proton dose and the secondary dose plotted separately for the E^{-3} spectrum and for one-dimensional cases. It is seen that the nuclear data assumptions made here lead to a relatively small secondary radiation dose, even with "upper limit" inelastic scatter cross sections. It should be noted that for steeper primary spectra the primary absorption is greater, so that the secondary dose is a larger fraction of the primary than for spectra having smaller n values.[9] However, the secondary dose is clearly a small fraction of the primary proton dose for tissue thicknesses up to 20 gm/cm^2 and aluminum shields of up to 10 gm/cm^2, for typical space proton spectra. Further, the solid angle subtended by tissue thickness greater than 20 gm/cm^2 around the deepest body points considered (GUT, WAIST 8) totals only about 20 percent[3], and it is even less for most radiosensitive organs. Thus the total dose to these organs is essentially equal to the primary proton dose, computed by Eq. 8, for feasibly thin external aluminum shields.

Tables 3 through 7 show the total doses at each of the body points considered for a variety of aluminum shells for the E^{-2}, E^{-3}, E^{-4}, E^{-5}, and Van Allen spectra, respectively. The units are tissue rad per incident isotropic proton/cm^2 having $E > 100$ Mev. These values utilize the three-dimensional human geometry analyses, Eq. 8, and the solid-line cross section data of Fig. 3. The nuclear data used are thus reasonable composites of published experimental information.

In addition to the twelve body points with only external shell shielding, four special cases are listed. In the case WAIST 4S, a shielding chair of either 2 gm/cm^2 or 4 gm/cm^2 polyethylene is considered with three outer aluminum shell values. The line labelled FEMUR B is a 72-region case in which the structure of the bone was considered. The line labelled EYE G is a case in which 0.25 cm of lead glass was added to the zero tissue thickness region of the EYE analysis; that is, to the front of the eye lens. The case CHEST 2

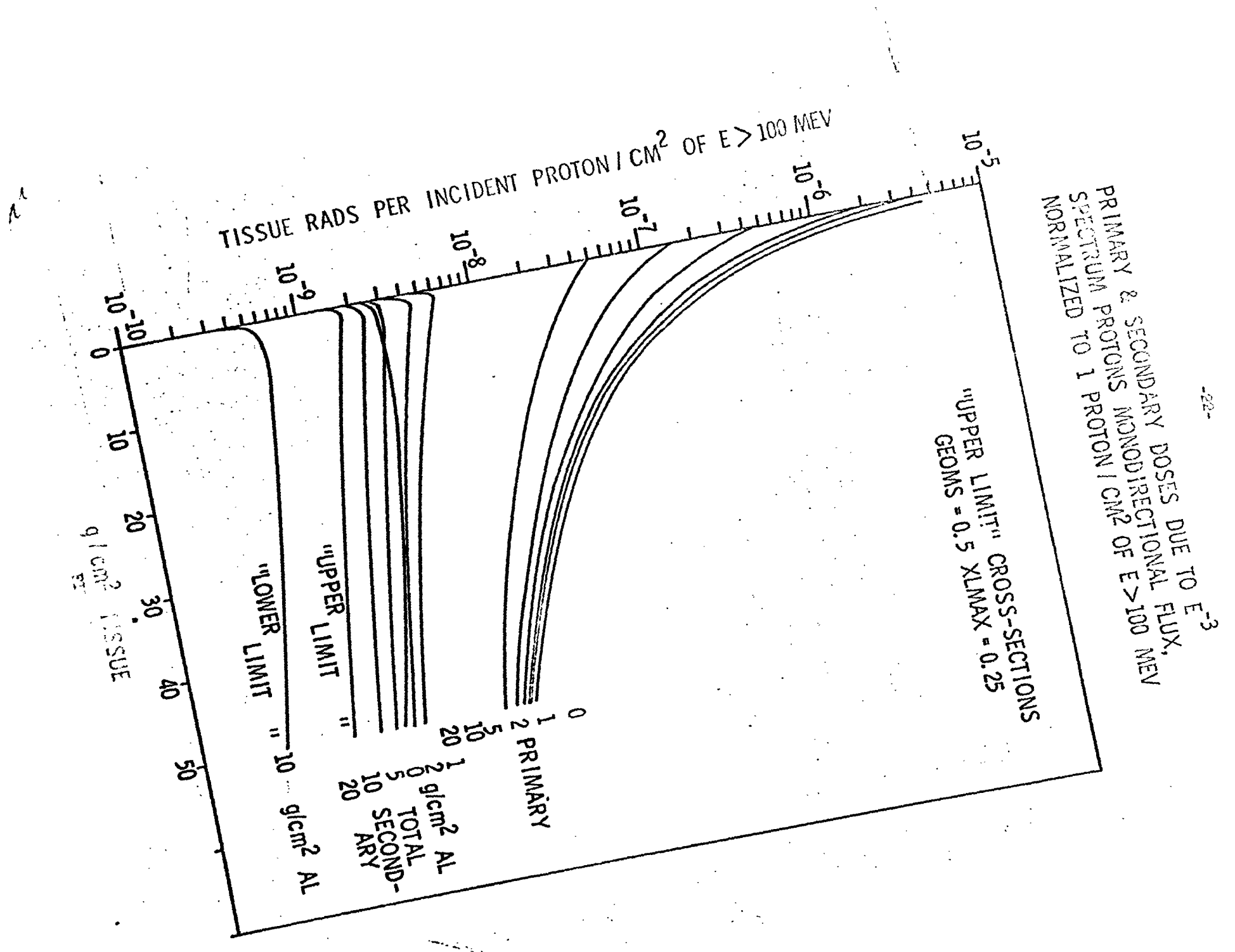
TISSUE RADS PER INCIDENT PROTON / CM2 OF E > 100 MEV
10-5
10-6
10-7
10-8
10-9
10-10
0
10
20
30
40
50
g / cm2 TISSUE
"UPPER LIMIT" CROSS-SECTIONS
GEOMS = 0.5 XLMAX = 0.25
PRIMARY & SECONDARY DOSES DUE TO E-3
SPECTRUM PROTONS MONODIRECTIONAL FLUX,
NORMALIZED TO 1 PROTON / CM2 OF E > 100 MEV
0
1
2 PRIMARY
5
10
20
1
2
5
10
20 g/cm2 AL
TOTAL SECONDARY
"UPPER LIMIT "
"LOWER LIMIT " 10 g/cm2 AL

Table 3. Doses at Specific Body Points Due to Incident Isotropic Proton Flux with n = 2 Spectrum, for Various Aluminum Shell Shield Thicknesses (rads per proton/cm^2 of E > 100 Mev)

Body Points	Aluminum Shell Thickness (gm/cm^2)						
	0	1	2	4	6	8	10
GUT	5.4×10^{-8}	5.1×10^{-8}	4.8^{-8}	4.3×10^{-8}	3.9×10^{-8}	3.6×10^{-8}	3.3×10^{-8}
CHEST 0	3.0×10^{-6}	6.5×10^{-7}	3.3×10^{-7}	1.7×10^{-7}	1.2×10^{-7}	8.9×10^{-8}	7.3×10^{-8}
CHEST 2	1.3×10^{-7}	1.1×10^{-7}	9.2×10^{-8}	7.2×10^{-8}	6.1×10^{-8}	5.2×10^{-3}	4.6×10^{-8}
CHEST 2L (Sternum)	1.4×10^{-7}	1.2×10^{-7}	1.0×10^{-7}	8.0×10^{-8}	6.7×10^{-8}	5.8×10^{-8}	5.1×10^{-8}
BK 2 (Spinal Column)	1.4×10^{-7}	1.1×10^{-7}	9.5×10^{-8}	7.5×10^{-8}	6.2×10^{-8}	5.4×10^{-8}	4.7×10^{-8}
WAIST 0	2.4×10^{-6}	5.2×10^{-7}	2.7×10^{-7}	1.4×10^{-7}	1.0×10^{-7}	7.9×10^{-8}	6.5×10^{-8}
WAIST 1	1.3×10^{-7}	1.1×10^{-7}	9.5×10^{-8}	7.5×10^{-8}	6.2×10^{-8}	5.4×10^{-8}	4.7×10^{-8}
WAIST 4	7.6×10^{-8}	6.9×10^{-8}	6.3×10^{-8}	5.4×10^{-8}	4.8×10^{-8}	4.3×10^{-8}	3.9×10^{-8}
WAIST 6	6.1×10^{-8}	5.7×10^{-8}	5.3×10^{-8}	4.7×10^{-8}	4.2×10^{-8}	3.8×10^{-8}	3.5×10^{-8}
WAIST 8	5.5×10^{-8}	5.2×10^{-8}	4.9×10^{-8}	4.3×10^{-8}	3.9×10^{-8}	3.6×10^{-8}	3.3×10^{-8}
WAIST 4S (2 gm/cm^2 CH_2 chair)	6.6×10^{-8}		5.6×10^{-8}		4.4×10^{-8}		
(4 gm/cm^2 CH_2 chair)	5.9×10^{-8}		5.1×10^{-8}		4.4×10^{-8}		
FEMUR	8.0×10^{-8}	7.2×10^{-8}	6.6×10^{-8}	5.7×10^{-8}	5.0×10^{-8}	4.5×10^{-8}	4.1×10^{-8}
FEMUR B	8.0×10^{-8}	7.3×10^{-8}	6.7×10^{-8}	5.8×10^{-8}	5.2×10^{-8}	4.7×10^{-8}	4.5×10^{-8}
EYE	2.5×10^{-6}	5.6×10^{-7}	3.1×10^{-7}	1.7×10^{-7}	1.2×10^{-7}	9.1×10^{-8}	7.5×10^{-8}
EYE G (2.5 mm glasses)	1.1×10^{-6}	4.4×10^{-7}	2.6×10^{-7}				

Table 4. Doses at Specific Body Points Due to Incident Isotropic Proton Flux with n = 3 Spectrum, for Various Aluminum Shell Shield Thicknesses (rads per proton/cm^2 of E > 100 Mev)

Body Points	Aluminum Shell Thickness (gm/cm^2)						
	0	1	2	4	6	8	10
GUT	5.6×10^{-8}	5.0×10^{-8}	4.6×10^{-8}	3.9×10^{-8}	3.4×10^{-8}	2.9×10^{-8}	2.6×10^{-8}
CHEST 0	2.8×10^{-8}	3.5×10^{-6}	1.2×10^{-6}	3.9×10^{-7}	2.1×10^{-7}	1.3×10^{-7}	9.5×10^{-8}
CHEST 2	2.8×10^{-7}	2.0×10^{-7}	1.5×10^{-7}	9.9×10^{-8}	7.3×10^{-8}	5.6×10^{-8}	4.6×10^{-8}
CHEST 2L (Sternum)	2.9×10^{-7}	2.1×10^{-7}	1.6×10^{-7}	1.1×10^{-7}	8.2×10^{-8}	6.4×10^{-5}	5.2×10^{-8}
BK 2 (Spinal Column)	3.0×10^{-7}	2.1×10^{-7}	1.6×10^{-7}	1.0×10^{-7}	7.6×10^{-8}	5.8×10^{-8}	4.7×10^{-8}
WAIST 0	2.2×10^{-5}	2.7×10^{-6}	9.2×10^{-7}	3.2×10^{-7}	1.7×10^{-7}	1.1×10^{-7}	8.1×10^{-8}
WAIST 1	2.9×10^{-7}	2.0×10^{-7}	1.6×10^{-7}	1.0×10^{-8}	7.5×10^{-8}	5.8×10^{-8}	4.7×10^{-8}
WAIST 4	1.1×10^{-7}	9.0×10^{-8}	7.7×10^{-8}	5.9×10^{-8}	4.8×10^{-8}	4.0×10^{-8}	3.4×10^{-8}
WAIST 6	7.2×10^{-8}	6.4×10^{-8}	5.7×10^{-8}	4.6×10^{-8}	3.9×10^{-8}	3.3×10^{-8}	2.9×10^{-8}
WAIST 8	6.0×10^{-8}	5.3×10^{-8}	4.8×10^{-8}	4.0×10^{-8}	3.4×10^{-8}	3.0×10^{-8}	2.6×10^{-8}
WAIST 4S (2 gm/cm^2 CH_2 chair)	8.3×10^{-8}		6.3×10^{-8}		4.1×10^{-8}		
WAIST 4S (4 gm/cm^2 CH_2 chair)	7.0×10^{-8}		5.4×10^{-8}		3.7×10^{-8}		
FEMUR	1.1×10^{-7}	9.3×10^{-8}	8.0×10^{-8}	6.3×10^{-8}	5.1×10^{-8}	4.2×10^{-8}	3.6×10^{-8}
FEMUR B	1.1×10^{-7}	9.4×10^{-8}	8.2×10^{-8}	6.4×10^{-8}	5.3×10^{-8}	4.4×10^{-8}	3.8×10^{-8}
EYE	2.2×10^{-5}	2.9×10^{-6}	1.0×10^{-6}	3.6×10^{-7}	2.0×10^{-7}	1.3×10^{-7}	9.6×10^{-8}
EYE G (2.5 mm glasses)	7.1×10^{-6}	1.9×10^{-6}	8.3×10^{-7}				

Table 5. Doses at Specific Body Points Due to Incident Isotropic Proton Flux with n = 4 Spectrum, for Various Aluminum Shell Shield Thicknesses (rads per proton/cm^2 or E > 100 Mev)

Body Points	Aluminum Shell Thickness (gm/cm^2)						
	0	1	2	4	6	8	10
GUT	6.3×10^{-8}	5.6×10^{-8}	4.7×10^{-8}	3.8×10^{-8}	3.1×10^{-8}	2.6×10^{-8}	2.0×10^{-8}
CHEST 0	2.2×10^{-4}	1.7×10^{-5}	3.9×10^{-6}	8.4×10^{-7}	3.3×10^{-7}	1.7×10^{-7}	1.1×10^{-7}
CHEST 2	5.7×10^{-7}	3.4×10^{-7}	2.3×10^{-7}	1.3×10^{-7}	8.1×10^{-8}	5.6×10^{-8}	4.4×10^{-8}
CHEST 2L (Sternum)	5.9×10^{-7}	3.6×10^{-7}	2.4×10^{-7}	1.4×10^{-7}	8.8×10^{-8}	6.2×10^{-8}	4.7×10^{-8}
BK 2 (Spinal Column)	6.0×10^{-7}	3.6×10^{-7}	2.5×10^{-7}	1.4×10^{-7}	8.5×10^{-8}	6.1×10^{-8}	4.7×10^{-8}
WAIST 0	1.6×10^{-4}	1.3×10^{-5}	2.8×10^{-6}	6.3×10^{-7}	2.6×10^{-7}	1.4×10^{-7}	9.4×10^{-8}
WAIST 1	5.7×10^{-7}	3.5×10^{-7}	2.4×10^{-7}	1.4×10^{-7}	8.6×10^{-8}	6.0×10^{-8}	4.5×10^{-8}
WAIST 4	1.5×10^{-7}	1.1×10^{-7}	8.9×10^{-8}	6.2×10^{-8}	4.6×10^{-8}	3.5×10^{-8}	2.9×10^{-8}
WAIST 6	8.3×10^{-8}	7.0×10^{-8}	5.8×10^{-8}	4.3×10^{-8}	3.4×10^{-8}	2.7×10^{-8}	2.3×10^{-8}
WAIST 8	6.4×10^{-8}	5.5×10^{-8}	4.7×10^{-8}	3.6×10^{-8}	3.0×10^{-8}	2.4×10^{-8}	2.0×10^{-8}
WAIST 4S (2 gm/cm^2 CH_2 chair)	1.0×10^{-7}		6.6×10^{-8}		3.8×10^{-8}		
(4 gm/cm^2 CH_2 chair)	8.3×10^{-8}		5.7×10^{-8}		3.3×10^{-8}		
FEMUR	1.4×10^{-7}	1.2×10^{-7}	8.9×10^{-8}	6.3×10^{-8}	4.8×10^{-8}	3.8×10^{-8}	3.1×10^{-8}
FEMUR B	1.3×10^{-7}	1.1×10^{-7}	8.9×10^{-8}	6.5×10^{-8}	5.0×10^{-8}	3.9×10^{-8}	3.1×10^{-8}
EYE	1.7×10^{-4}	1.4×10^{-5}	3.0×10^{-6}	6.1×10^{-7}	3.1×10^{-7}	1.8×10^{-7}	1.2×10^{-7}
EYE G (2.5 mm glasses)	3.9×10^{-5}	8.4×10^{-6}	2.3×10^{-6}				

Table 6. Doses at Specific Body Points Due to Incident Isotropic Proton Flux with n = 5 Spectrum, for Various Aluminum Shell Thicknesses (rads per proton/cm^2 of E > 100 Mev)

Body Points	Aluminum Shell Thickness (gm/cm^2)						
	0	1	2	4	6	8	10
GUT	5.8×10^{-8}	5.4×10^{-8}	4.2×10^{-8}	3.3×10^{-8}	2.5×10^{-8}	2.2×10^{-8}	1.9×10^{-8}
CHEST 0	1.6×10^{-3}	7.8×10^{-5}	1.0×10^{-5}	1.4×10^{-6}	4.8×10^{-7}	2.3×10^{-7}	1.2×10^{-7}
CHEST 2	1.1×10^{-6}	6.2×10^{-7}	3.4×10^{-7}	1.6×10^{-7}	8.7×10^{-8}	5.9×10^{-8}	4.2×10^{-8}
CHEST 2L (Sternum)	1.1×10^{-6}	6.0×10^{-7}	3.6×10^{-7}	1.7×10^{-7}	9.7×10^{-8}	6.5×10^{-8}	4.7×10^{-8}
BK 2 (Spinal Column)	1.1×10^{-6}	6.0×10^{-7}	3.7×10^{-7}	1.7×10^{-7}	1.0×10^{-7}	6.4×10^{-8}	4.9×10^{-8}
WAIST 0	1.2×10^{-3}	6.0×10^{-5}	7.9×10^{-6}	1.1×10^{-6}	3.8×10^{-7}	1.8×10^{-7}	1.0×10^{-7}
WAIST 1	1.0×10^{-6}	5.4×10^{-7}	3.3×10^{-7}	1.5×10^{-7}	8.9×10^{-8}	5.8×10^{-8}	4.1×10^{-8}
WAIST 4	1.8×10^{-7}	1.3×10^{-7}	9.8×10^{-8}	6.3×10^{-8}	4.4×10^{-8}	3.3×10^{-8}	2.6×10^{-8}
WAIST 6	8.3×10^{-8}	5.7×10^{-8}	5.9×10^{-8}	4.1×10^{-8}	3.1×10^{-8}	2.5×10^{-8}	2.2×10^{-8}
WAIST 8	6.8×10^{-8}	5.9×10^{-8}	4.7×10^{-8}	3.3×10^{-8}	2.7×10^{-8}	2.2×10^{-8}	19.0×10^{-9}
WAIST 4S (2 gm/cm^2 CH_2 chair)	1.1×10^{-7}		6.7×10^{-8}		3.4×10^{-8}		
(4 gm/cm^2 CH_2 chair)	8.9×10^{-8}		5.4×10^{-8}		3.0×10^{-8}		
FEMUR	1.7×10^{-7}	1.4×10^{-7}	9.9×10^{-8}	6.3×10^{-8}	4.5×10^{-8}	3.4×10^{-8}	2.7×10^{-8}
FEMUR B	1.5×10^{-7}	1.3×10^{-7}	9.6×10^{-8}	6.4×10^{-8}	4.7×10^{-8}	3.7×10^{-8}	2.75×10^{-8}
EYE	1.2×10^{-3}	6.2×10^{-5}	8.3×10^{-6}	1.2×10^{-6}	4.2×10^{-7}	2.0×10^{-7}	1.1×10^{-7}
EYE G (2.5 mm glasses)	1.9×10^{-4}	3.7×10^{-5}	5.5×10^{-6}				

Table 7. Doses at Specific Body Points Due to Incident Isotropic Proton Flux with Van Allen Spectrum, for Various Aluminum Shell Shield Thicknesses (rads per proton/cm^2 of E > 40 Mev)

Body Points	Aluminum Shell Thickness (gm/cm^2)						
	0	1	2	4	6	8	10
GUT	3.1×10^{-8}	2.9×10^{-8}	2.8×10^{-8}	2.5×10^{-9}	2.3×10^{-8}	2.1×10^{-8}	1.9×10^{-8}
CHEST 0	3.8×10^{-7}	1.3×10^{-7}	1.0×10^{-7}	7.5×10^{-8}	6.0×10^{-8}	5.0×10^{-8}	4.2×10^{-8}
CHEST 2	6.0×10^{-8}	5.4×10^{-8}	4.9×10^{-8}	4.1×10^{-8}	3.5×10^{-8}	3.0×10^{-8}	2.7×10^{-8}
CHEST 2L (Sternum)	6.7×10^{-8}	6.0×10^{-8}	5.4×10^{-8}	4.6×10^{-8}	3.9×10^{-8}	3.4×10^{-8}	3.0×10^{-8}
BK 2 (Spinal Column)	6.2×10^{-8}	5.6×10^{-8}	5.0×10^{-8}	4.2×10^{-8}	3.6×10^{-8}	3.1×10^{-8}	2.7×10^{-8}
WAIST 0	3.1×10^{-7}	1.2×10^{-7}	9.4×10^{-8}	6.9×10^{-8}	5.5×10^{-8}	4.5×10^{-8}	3.8×10^{-8}
WAIST 1	6.4×10^{-8}	5.7×10^{-8}	5.2×10^{-8}	4.3×10^{-8}	3.7×10^{-8}	3.1×10^{-8}	2.8×10^{-8}
WAIST 4	4.4×10^{-8}	4.0×10^{-8}	3.7×10^{-8}	3.2×10^{-8}	2.8×10^{-8}	2.5×10^{-8}	2.3×10^{-8}
WAIST 6	3.6×10^{-8}	3.3×10^{-8}	3.1×10^{-8}	2.7×10^{-8}	2.4×10^{-8}	2.2×10^{-8}	2.0×10^{-8}
WAIST 8	3.2×10^{-8}	3.0×10^{-8}	2.8×10^{-8}	2.5×10^{-8}	2.3×10^{-8}	2.1×10^{-8}	1.9×10^{-8}
WAIST 4S (2 gm/cm^2 CH_2 chair)	3.8×10^{-8}		3.3×10^{-8}		2.5×10^{-8}		
WAIST 4S (4 gm/cm^2 CH_2 chair)	3.4×10^{-8}		3.0×10^{-8}		2.4×10^{-8}		
FEMUR	4.5×10^{-8}	4.2×10^{-8}	3.8×10^{-8}	3.3×10^{-8}	2.9×10^{-8}	2.6×10^{-8}	2.4×10^{-8}
FEMUR B	4.7×10^{-8}		4.0×10^{-8}		3.0×10^{-8}		
EYE	3.3×10^{-7}	1.3×10^{-7}	1.0×10^{-7}	7.7×10^{-8}	6.2×10^{-8}	5.1×10^{-8}	4.3×10^{-8}
EYE G (2.5 mm glasses)	1.5×10^{-7}	1.0×10^{-7}	8.6×10^{-8}				

PRIMARY PROTON DOSE vs LATERAL WAIST DEPTH FOR VARIOUS ALUMINUM SHELL SHIELD THICKNESS. E^{-3} SPECTRUM

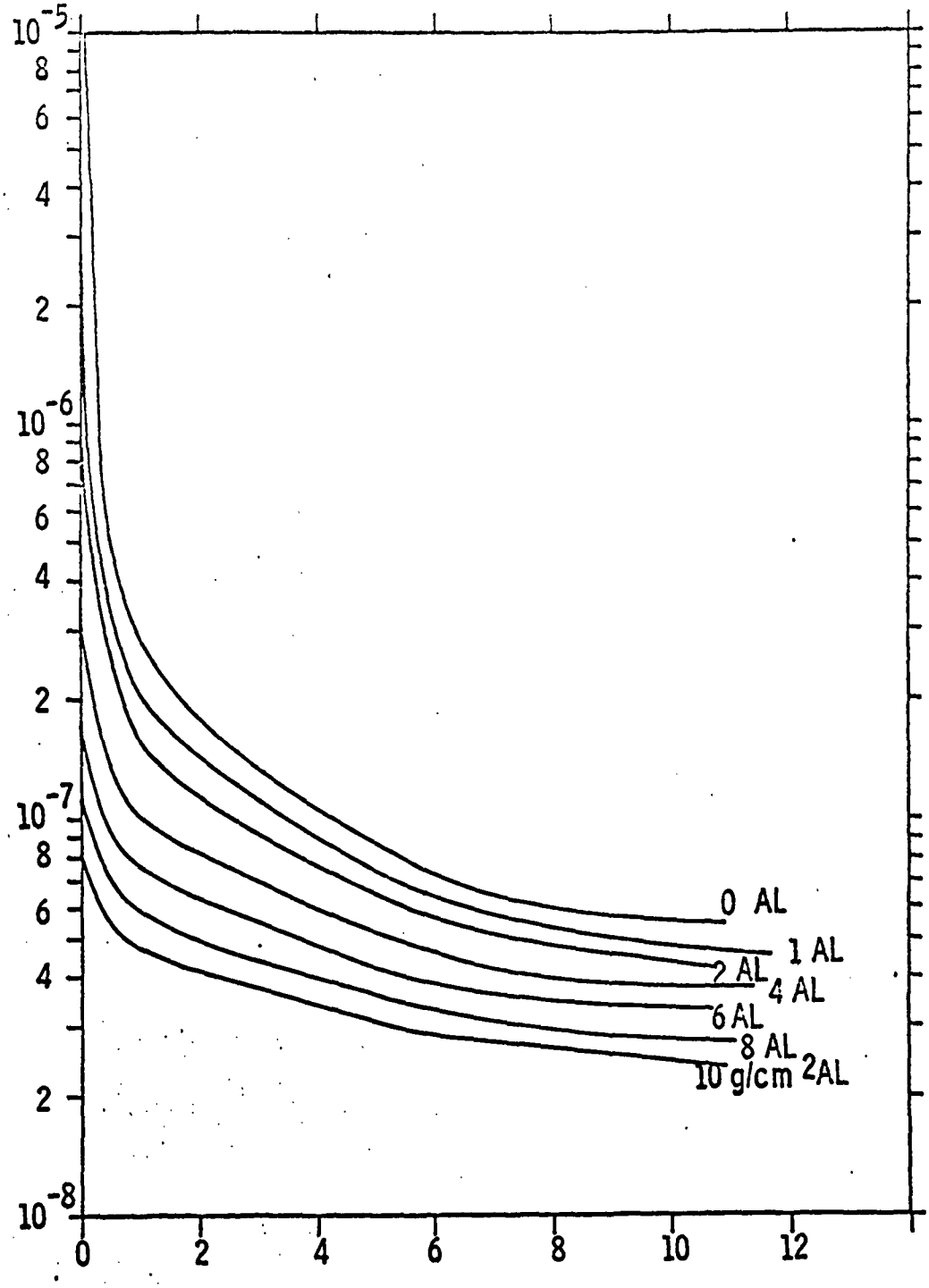

FIGURE 7

ignores air in the lungs and bilateral asymmetry due to the heart; CHEST 2L takes these into account. It is seen from Tables 3 through 7 that to take account of lung air or bone structure is hardly worth the extra analysis effort and computing time for the proton dose.

The depth-dose pattern in the human body is felt to be of special significance[13] and so the doses at points laterally along the waist are plotted in Fig. 7 to show the representative pattern. It is seen from Fig. 7 and the tabulated values that a midline dose of 15 to 30 percent the skin dose is typical, dpending on shielding and spectrum in obvious ways.

Because of the normalization used in the values reported here, they may readily be applied to environment data. If a trajectory is known, the trapped proton flux of $E > 40$ Mev may be computed and integrated over the orbit.[14] If a specific solar flare proton event is estimated to have a spectrum denoted by n and size in protons/cm^2, both parameters integrated over the whole event, (or instantaneous flux in protons/cm^2-sec), then total dose (or dose rate) may be determined to any of the body points. An estimated flare size-probability curve can be converted to significant dose-probability[15] using these data and vehicle shielding assumptions. By simple descriptive geometry techniques and the codes here reported, the shielding required in specific vehicle designs may be computed so as to maintain a desired lower probability limit for specified organ tolerance dose.

---

13. K. L. Jackson, The Lethal Effectiveness of a Solar Flare-type Dose Distribution Delivered to the Rat, this symposium.

14. F. C. Perry, Proton Fluxes Along Trajectories Through the Inner Van Allen Belt, this symposium.

15. E. L. Chupp, D. L. Dye, B. W. Mar, L. O. Oncley, and R. W. Williams, Analysis of Solar-Flare Hazards to Manned Space Systems, The Boeing Company, D2-11608 (1961)